Published in
Proceedings of the IEEE 98, issue 7, 1255-1268, 2010
which should be used for any reference to this work

ZnO Devices and Applications: A Review of Current Status and Future Prospects

The possible importance of zinc-oxide-based optoelectronic devices is reviewed in this paper, which places special emphasis on the need to achieve p-type ZnO.

By Ümit Özgür, *Member IEEE*, Daniel Hofstetter, and Hadis Morkoç

ABSTRACT | ZnO is an attractive material for applications in electronics, photonics, acoustics, and sensing. In optical emitters, its high exciton binding energy (60 meV) gives ZnO an edge over other semiconductors such as GaN if reproducible and reliable *p*-type doping in ZnO were to be achieved, which currently remains to be the main obstacle for realization of bipolar devices. On the electronic side, ZnO holds some potential in transparent thin film transistors (TFTs) owing to its high optical transmittivity and high conductivity. Among the other promising areas of application for ZnO are acoustic wave devices, due to large electromechanical coupling in ZnO, and devices utilizing nanowires/nanorods such as biosensors and gas sensors and solar cells, since it is relatively easy to produce such forms of ZnO nanostructures, which have good charge carrier transport properties and high crystalline quality. Despite the significant progress made, there is still a number of important issues that need to be resolved before ZnO can be transitioned to commercial use, not to mention the stiff competition it is facing with GaN, which is much more mature in terms of devices. In this paper, recent progress in device applications of ZnO is discussed and a review of critical issues for realization of ZnO-based devices is given.

KEYWORDS | Distributed feedback lasers; light-emitting diodes (LEDs); nanostructure devices; thin film transistors (TFTs); transparent oxides; zinc oxide

Ü. Özgür and **H. Morkoç** are with the Department of Electrical and Computer Engineering, Virginia Commonwealth University, Richmond, VA 23284 USA (e-mail: uozgur@vcu.edu; hmorkoc@vcu.edu).
D. Hofstetter is with the Institute of Physics, University of Neuchatel, 2009 Neuchatel, Switzerland (e-mail: Daniel.Hofstetter@unine.ch).

I. INTRODUCTION

In many respects, ZnO is considered to be an alternate to GaN for device applications owing to its relatively low production cost and superior optical properties. However, reproducible and stable *p*-type doping remains to be the most daunting obstacle to producing bipolar ZnO-based devices. It is a given that GaN device technology is much more mature as GaN-based very high-performance electronic and optical devices have already been commercialized. GaN-based power field effect transistors (FETs) are capable of producing over 800 W of continuous-wave (CW) power in the communication band, light-emitting diodes (LEDs) have created a large market with emphasis in performance being on the efficiency although they are already more efficient than even the fluorescent bulbs, and blue lasers are already used in game consoles and high-definition video players. The same, however, cannot yet be said about ZnO particularly when its potential applications overlap considerably with those of GaN. On the electronic side, the relatively low mobility of ZnO as compared to GaN and nearly four times stronger electron–phonon coupling together with relatively low thermal conductivity are serious shortcomings for ZnO. However, transparent thin film transistors (TFTs) built from poly-ZnO appear to hold some potential. Furthermore, the potential worldwide shortage of indium in the face of growing demand for indium tin oxide (ITO) seems to be stimulating the exploration of ZnO-based transparent oxides, which if successful, could become a huge application area. It remains to be seen, however, as to how competitive ZnO would be with the existing technologies. On the optical device front, ZnO needs to show high *p*-type conductivity along with high-quality heterojunctions for realization of competitive light emitters. One major advantage of ZnO is its high 60-meV

exciton binding energy compared to 25 meV of GaN. If lasers utilizing excitonic transitions were to be built, ZnO would have an advantage over GaN provided that *p*-type conductivity is obtained and other necessary processing capabilities are developed for ZnO. Another promising application area of ZnO is acoustic wave devices owing to its large electromechanical coupling, particularly along the *c*-direction. Further yet, ZnO appears to be well suited for producing nanostructures, which may be used for devices. A significant part of the recent research in the field of ZnO-based devices and applications deals with ZnO nanostructures (nanowires, nanobelts, etc.) and their integration with the mainstream semiconductor materials—such as Si, GaN, and organic semiconductors. ZnO nanowires have attracted a lot of attention due to their good charge carrier transport properties and high crystalline quality [1]–[3]. Such 1-D systems have unique properties that make them potentially attractive for nanoscale devices [LEDs, lasers, photodetectors, chemical/biosensors, and surface acoustic wave (SAW) devices], which have been intensively investigated [4]–[7].

In this paper, device applications of ZnO are discussed and a critical review of the recent progress in this field is given. First, optical devices, such as light-emitting diodes (LEDs), optically pumped lasers, and transparent thin films transistors based on ZnO are reviewed. This is followed by a discussion of ZnO piezoelectric devices. Finally, gas/biosensor and solar cell applications exploiting the unique properties of ZnO nanostructures are discussed.

II. OPTICAL DEVICES

Reiterating, ZnO is considered as a potentially attractive material for light-emitting devices emitting in the ultraviolet (UV) region, because of its large exciton binding energy (60 meV). Since reproducible *p*-type ZnO has not yet been developed widespread fabrication of ZnO *p*–*n* homojunction-based LEDs has not been possible. In the interim, *n*-type ZnO on other available and comparable *p*-type materials was used for at least investigating the particulars of junctions participated by ZnO. This subject has seen a great deal of activity, and heterojunctions have been realized using various *p*-type materials such as Si, GaN, AlGaN, $SrCu_2O_2$, NiO, ZnTe, Cu_2O, CdTe, SiC, diamond, $ZnRh_2O_4$, and ZnO/GaAs. Some details of these heterostructures concerning their growth and properties can be found in [8] and [9]. In general, electroluminescence (EL) under forward bias was observed to be weak, while in some cases the *p*–*n* heterojunctions were considered for uses as ultraviolet photodetectors (PDs). If studies on radiation hardness of ZnO hold true [10], ZnO-based PDs in and of themselves could have superior resistance to ionizing radiation and high-energy particles. In the absence of *p*–*n* junctions, EL properties of ZnO have also been exploited by fabricating metal–insulator–semiconductor (MIS) structures which do not require *p*-type ZnO [11].

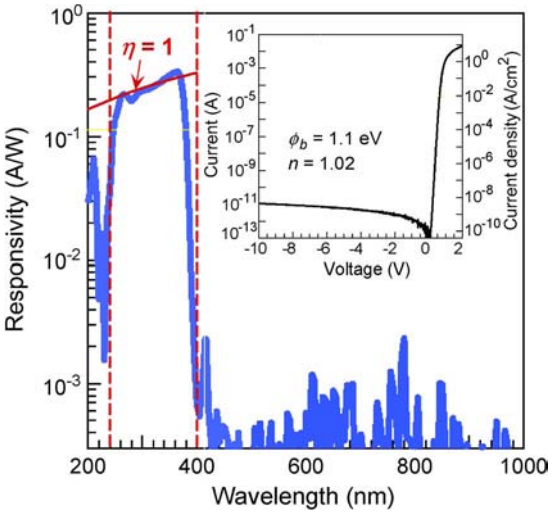

Fig. 1. ***Responsivity of a PEDOT : PSS/ZnO Schottky photodiode at zero bias as a function of the incident photon wavelength. The vertical dashed lines mark the onsets of absorption in PEDOT: PSS (left) and ZnO (right). The inset shows the typical IV characteristics in dark. (After Nakano et al. [12].)***

Schottky diodes based on ZnO have also been implemented as high-efficiency UV photodetectors. In one particular study [12], a spin coated transparent and conducting polymer [poly(3,4-ethylenedioxythiophene) poly(styrenesulfonate) (PEDOT : PSS)] has been used as a Schottky contact on hydrothermally grown Zn-polar single crystal ZnO (Tokyo Denpa). Schottky diodes of $500 \times 500\ \mu m^2$ in size exhibited current densities of $\sim 4 \times 10^{-9}$ A/cm^2 at -10 V and ~ 10 A/cm^2 at $+2$ V (ideality factor $n = 1.02$ and Schottky barrier height $\phi_b = 1.1$ eV). Under illumination and at zero bias, the photodiodes attained a significantly large responsivity of 0.3 A/W at 370 nm corresponding to unity quantum efficiency, and a UV/visible rejection ratio of about 10^3 as shown in Fig. 1. Such structures that do not involve *p*-type ZnO are promising for application in UV detection.

ZnO is also extremely attractive as a transparent contact layer due to its high conductivity and transparency in addition to its low cost (needs to be lowered further), nontoxicity, and relatively low deposition temperature. In general, PDs based on other semiconductors with ZnO transparent window layers would have a significant advantage over the ITO window varieties because the transparency of ZnO at 450 nm is more than that of ITO (~90%), and ZnO is also expected to offer lower resistance.

A. Light-Emitting Diodes

One of the first if not the first ZnO-based hybrid heterostructure LEDs was fabricated by Drapak [13] in 1968 who used Cu_2O as a *p*-type layer. In all the other hybrid structures that followed, the emission observed under forward bias either originated in the *p*-type layer, or

showed a very weak contribution at the ZnO band edge corresponding to extremely small external quantum efficiencies. When *p*-AlGaN was used to favor hole injection into ZnO thereby promoting emission in that material, strong EL peaking at ~390 nm due to excitonic recombination within ZnO has been observed [14], [15]. Although these results show that *p*-AlGaN is a good candidate for fabricating efficient hybrid heterostructure LEDs with ZnO active layers, all ZnO-based LEDs incorporating stable *p*-ZnO are needed for light emitters to compete with those based on nitrides.

Reports on all ZnO-based light-emitting devices have also started to appear [16], [17] as *p*-type ZnO began to become available. However, production of stable and device-quality *p*-type ZnO has not been realized despite a large number of publications reporting successful demonstration of *p*-type as discussed in detail in [18]. Incorrect interpretation of the van der Pauw–Hall measurements has been suggested [19] as one of the reasons for the controversial reports of *p*-type conduction in ZnO. In wide bandgap semiconductors doped with a high density of acceptor-type impurities, localization is an endemic problem: carriers are trapped and cannot follow the Lorentz force and the electric force induced by the low fields employed in Hall measurements. High carrier concentrations in *p*-type ZnO, which are often reported in the literature, are caused by very low Hall voltages. Corresponding low-mobility values measured are usually indicative of strong localization in the material, which, if present, brings the applicability of conventional Hall measurements under question, particularly at low temperatures. Therefore, the interpretation of Hall effect measurements should be made very carefully.

For reliable *p*-type behavior, first high density of donor-type defects should be minimized and almost intrinsic nearly perfect single crystal ZnO films should be obtained, which is still considered a major challenge. Even when such an approach was adopted, to the extent possible nitrogen doping resulted in very low *p*-doping concentration ($\sim 10^{16}$ cm^{-3}) [17], though recent first principles calculations suggest that nitrogen is a deep acceptor and cannot lead to hole conductivity [20]. Under such conditions, injection from the highly doped *n*-type ZnO to the lightly doped *p*-type ZnO is dominant and the recombination takes place primarily in the *p*-type ZnO, as shown in Fig. 2. This degrades the recombination efficiency as the quality of the *p*-type material is inferior. The EL emission coincides with the PL band at 440 nm which is thought to represent the donor–acceptor pair (DAP) recombination in *p*-type ZnO. To circumvent this problem, the *p*-doping level must be increased ($> 10^{18}$ cm^{-3}).

Near-bandedge EL has also been observed from ZnO homojunction LED structures fabricated using phosphorous-doped p-ZnO on gallium-doped n-ZnO grown by radio frequency (RF) sputtering on *c*-sapphire [21]. The *p*-ZnO layer was reported to have a questionably high hole concentration of 1.0×10^{19} cm^{-3} but a mobility of only 1 cm^2/V-s after rapid thermal annealing at 800 °C in N_2 ambient for 5 min. As shown in Fig. 3, UV emission was evident at 380 nm at room temperature. By inserting 40-nm-thick $Mg_{0.1}Zn_{0.9}O$ barrier layers with a 40-nm-thick *n*-ZnO layer in between near the *p*–*n* junction, the carrier recombination was confined in the *n*-type ZnO layer, which resulted in the suppression of the defect-related broad band

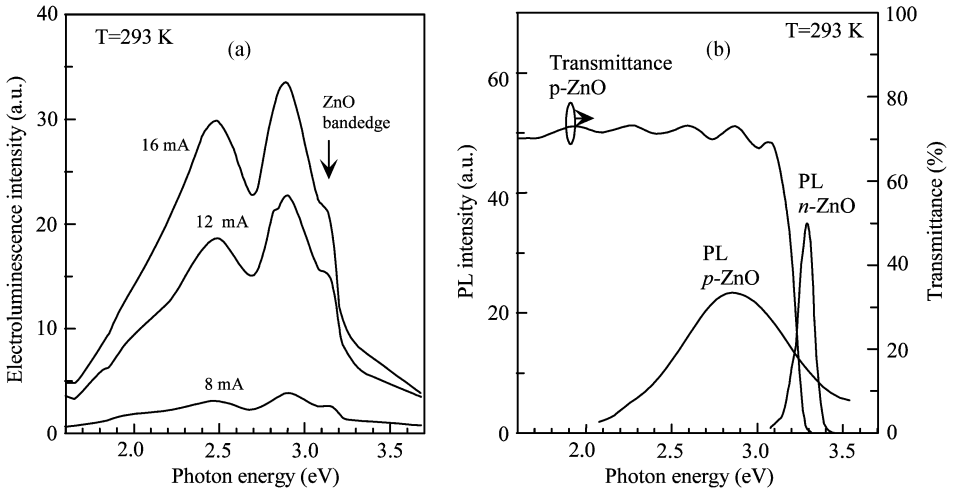

Fig. 2. ***(a) EL spectra of all ZnO p–n junction recorded at 293 K for dc forward bias currents of 8, 12, and 16 mA. The arrow indicates the absorption edge of p-type ZnO top layer. (b) PL spectra at 293 K of undoped and p-type ZnO layers (dotted lines) and transmission spectrum (broken line) of p-type ZnO layer. The EL emission is red shifted (440 nm) with respect to the bandedge and occurs where the PL emission is detected and is most likely associated with donor–acceptor-pair (DAP) transitions in the p-type ZnO layer. Thicknesses of the undoped and p-type films are 1 μm and 500 nm, respectively. (Courtesy of M. Kawasaki [17].)***

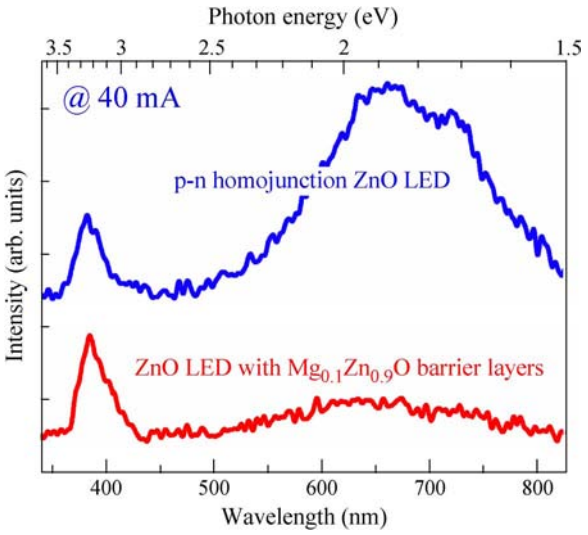

Fig. 3. *EL spectra from ZnO-based LEDs grown by RF sputtering with and without $Mg_{0.1}Zn_{0.9}O$ barrier layers measured at an operating current of 40 mA. (After Lim et al. [21].)*

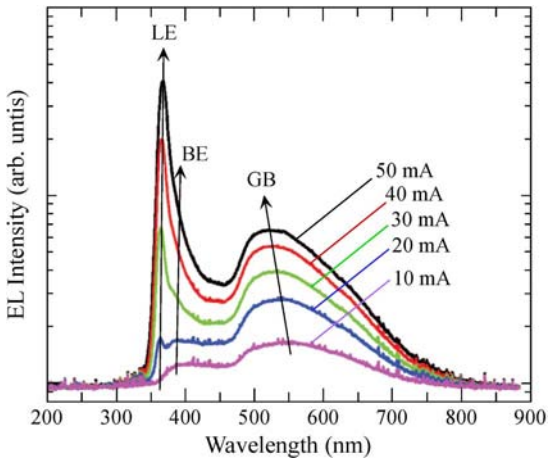

Fig. 4. *EL spectrum measured at room temperature for ZnO-based LED having seven BeZnO/ZnO QWs in the active layer. The primary spectral emission peak is located near 363 nm and arises from localized-exciton (LE) emissions in the QWs, while the secondary peak centered near 388 nm is from impurity-bound exciton emissions in ZnO. The green band (GB) blueshifts with increasing current injection. (After Ryu et al. [22].)*

centered at ∼650 nm and enhancement of the band edge emission by 55%.

ZnO-based LEDs were also fabricated using *p*-type arsenic-doped BeZnO and ZnO layers grown by hybrid beam deposition [22]. The hole concentrations in the *p*-type layers were reported to range from high 10^{16} cm^{-3} for BeZnO to mid-10^{17} cm^{-3} for ZnO. The active region was composed of seven undoped $Be_{0.2}Zn_{0.8}O$ (7 nm)/ZnO (4 nm) quantum wells (QWs). The turn on voltage was above 10 V, and UV EL peaks were observed at 363 and 388 nm at room temperature as shown in Fig. 4, which were attributed to localized excitons in the QWs and donor or acceptor bound excitons, respectively. The green band centered at ∼550 nm blue shifted with increasing current injection. The peak at 363 nm was the dominant spectral feature at current injection levels above 20 mA. Similar active regions were used to fabricate laser structures with $Be_{0.3}Zn_{0.7}O$ cladding layers [23]. Under pulsed current injection, sharp Fabry–Pérot oscillations were observed over the 3.21-eV emission peak, above a threshold current density of ∼420 A/cm^2. However, no further analysis of the cavity resonance mode separation was reported.

In terms of nanostructure devices, ZnO nanotips have been used to increase radiation outcoupling in the form of an improved passive light extraction layer in GaN light emitters [24]. As shown in Fig. 5(a), the Ga-doped ZnO (GZO) layer, which has the dual role of contact to *p*-GaN and optically transparent window, was deposited on top of conventional InGaN/GaN LED structures. Then, ZnO nanotips were grown on GZO coated GaN as a light extraction layer. In comparison with a conventional Ni/Au *p*-electrode GaN LED, the light emission efficiency was enhanced by a factor of ∼1.7 [Fig. 5(b)]. Enhancement in light extraction efficiency was explained by the interaction between the spontaneous emission from the GaN LED and ZnO nanostructures. The results represent one of the low-cost and large-scale fabrication methods for the integration of ZnO nanotips with GaN-based optoelectronic devices using epitaxial growth technologies without the need for e-beam lithography or etching. Even without the nanotips, GZO or Al-doped ZnO (AZO) coated GaN in place of ITO, which is used in all GaN-based LEDs, might turn out to be very lucrative in part fuelled by worldwide shortage of In.

B. Optically Pumped Lasers: Surface-Emitting ZnO DFB Laser

There are plenty of reports on UV lasing from ZnO-based materials and devices under optical pumping, for example, lasing from ZnO photonic crystals [25], [26] and random lasing from ZnO powder under certain pumping conditions [27]. ZnO-based microcavities promising for low-threshold surface-emitting polariton lasers are discussed in [28].

Yet another possibility for the realization of a surface-emitting laser is the use of an intracavity diffraction element. If the period of such a diffracting structure is carefully adapted to the emission wavelength and the effective refractive index of the device, distributed feedback (DFB) will occur. In the case of a second-order diffraction grating for optical feedback, the surface emission is at exactly 90° to the epitaxial layer plane [29]. In two recently demonstrated devices based on ZnO material, a third-order grating provided feedback. In the latter case, the optical output takes place at angles slightly different from 90°, but nevertheless the device can be

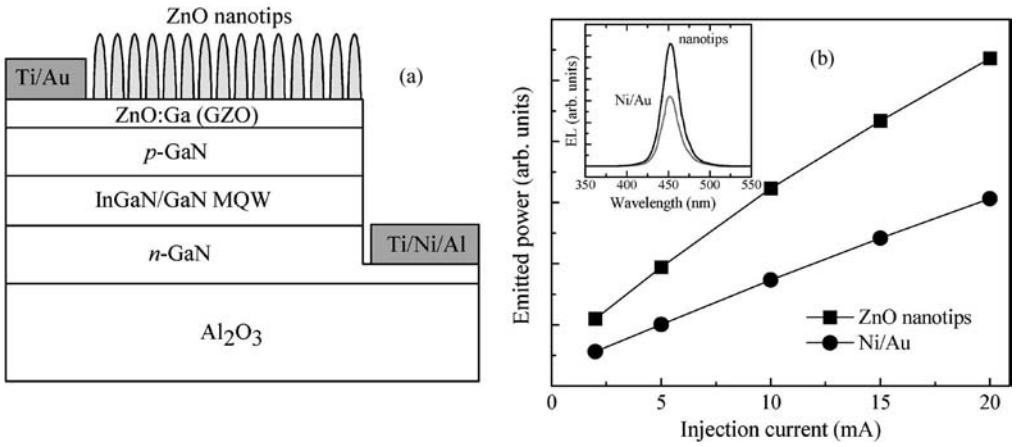

Fig. 5. *(a) Schematic of an integrated ZnO nanotip/GZO/GaN LED. (b) Light output power versus forward injection current for Ni/Au and ZnO nanotip/GZO/GaN LED; inset compares the EL spectra of Ni/Au p-contact GaN LED and ZnO nanotip/GZO/GaN LED at a forward current of 20 mA. (After Zhong et al. [24].)*

regarded as a surface emitter. In an optically pumped laser, the diffraction grating for DFB is typically etched directly into the active semiconductor material [30], [31]. Experiments have shown, however, that direct etching of a diffraction structure into a ZnO thin film is quite problematic. In order to circumvent difficulties with surface roughness, back reflections, and the etching process itself, a Si_3N_4 host layer for the grating needs to be deposited on the ZnO film. The thickness of this additional nitride layer has to be adapted to both the waveguide properties of the epitaxial layer stack and the desired coupling constant of the DFB laser.

One of the main purposes of optically pumped ZnO-based DFB lasers is to understand their spectral characteristics by investigation of their wavelength tuning behavior. In addition, the well-defined, line-shaped far-field distribution with precisely measurable emission angles allows an unambiguous confirmation of lasing action. Finally, the relatively large pumped volume of such a horizontal cavity surface emitter generates optical output powers which are large enough to be measured with standard photodetectors. This again is a considerable advantage for assessing the most important basic characteristics of the device [32]. All characteristics of optically pumped ZnO-based DFB lasers follow the expected behavior known since 1972 when Kogelnik and Shank published their seminal work on the coupled mode theory [33].

ZnO-based DFB lasers with thin film active regions have recently been implemented [34]. The active region consisted of a thin (5–10 nm) MgO nucleation layer followed by a nominally 200-nm-thick ZnO active region. A 120-nm-thick Si_3N_4 host layer for the grating deposited by plasma-enhanced chemical vapor deposition completed the waveguide structure. A schematic of the waveguide refractive index profile along with the vertical mode profile is shown in Fig. 6. It illustrates clearly that an optical overlap on the order of 7% can be achieved for the grating layer. By using a full 120-nm corrugation depth, this geometry results theoretically in a coupling strength of 400 cm^{-1} for a third-order diffraction grating.

Fabrication was based on holographic definition of the grating pattern with a period of 268 nm in a photoresist mask and subsequent transfer into the Si_3N_4 layer by reactive ion etching. The corrugation depth corresponds exactly to the thickness of the host layer, i.e., 120 nm. The inset of Fig. 6 shows a scanning electron microscope image of a small portion of the finished grating after etching into the Si_3N_4. Optical pumping was then performed at an angle of 70° to the surface normal in order to obtain a diffracted surface emission (±20° from the surface normal) going straight into a microscope objective. The pump source for this experiment was a pulsed nitrogen laser emitting at 337.1 nm; after focalization into a narrow stripe of 3.6×0.1 mm^2, its peak power density was 1.1 MW/cm^2.

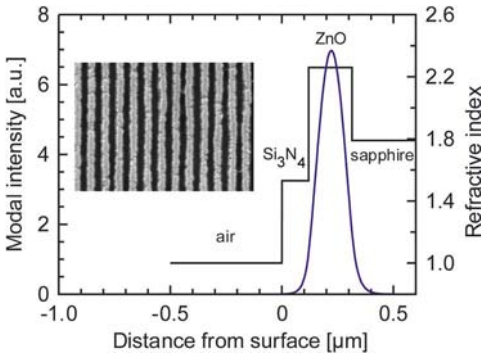

Fig. 6. *Waveguide simulation of an optically pumped ZnO DFB laser based on a thin film active region. The inset shows a small portion of the Bragg reflector acting as distributed feedback element.*

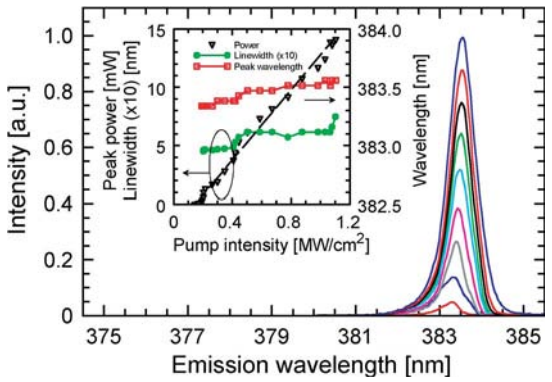

Fig. 7. ***Spectral characteristics of an optically pumped ZnO DFB laser at 220 K and different pump intensities (0.15, 0.25, 0.35, 0.45, 0.6, 0.8, 0.9, 1.0, 1.1 MW/cm^2). The inset shows peak power, peak wavelength, and linewidth as a function of pump power.***

From the microscope, the output beam entered a high-resolution grating spectrometer for spectral analysis.

The light output versus pump intensity curve was normalized by a careful measurement of the average intensities of both pump and output beams, and it exhibits a linear behavior above the lasing threshold as shown in Fig. 7. The center wavelength is at 383.5 nm and shifts slightly to longer wavelengths with increasing pump intensity (see inset of Fig. 7). Together with a larger linewidth at higher pump intensities, these observations prove clearly that thermal chirping is present in this material. The simulated effective refractive index of the waveguide ($n_{eff}^{th} = 2.181$) is in good agreement with that obtained from experiments ($n_{eff}^{ex} = 2.146$). These devices produced a maximum peak output power of 14 mW, and temperature tuned single-mode lasing could be observed up to around 270 K, with a performance maximum around 220 K. The low-temperature threshold intensity of the DFB laser was on the order of 120 kW/cm^2, which is reasonable considering the large pumped volume of the cavity. At threshold, the linewidth dropped from its luminescence value of 3.5 down to 0.4 nm. At temperatures around 120 K, an abrupt change of the laser wavelength occurred. Because of a hysteresis behavior of the emission wavelength seen under increasing and decreasing temperatures, we attribute this jump to lasing in a Bragg mode on one of the sides of the Bragg reflector's stopband. A comparison with the luminescence spectrum confirmed that indeed the single-mode lasing peak switched from the short to the long wavelength side of the gain maximum at this temperature. The size of the spectral stopband, i.e., the spectral separation between the two modes, finally allowed us to determine experimentally the coupling constant of the diffraction grating. Its value of 700 cm^{-1} agrees qualitatively with the computed value cited above.

In an attempt to reduce the pumping threshold of optically pumped ZnO-based DFB lasers, multi-QW active regions have been employed [35]. The basic fabrication concept resembles that used for the thin film devices described above, however, the exact realization is nevertheless subject to several important changes. Because of the lower refractive index of Mg-containing MgZnO compounds, the thicknesses and compositions of a waveguide using a QW active region need to be adapted. The epitaxial growth was initiated with a 20-nm-thick ZnO buffer, followed by a 400-nm $Mg_{0.3}Zn_{0.7}O$ lower cladding, a 30-nm $Mg_{0.2}Zn_{0.8}O$ lower waveguide layer, a nominally 93-nm-thick active region, and another 30-nm $Mg_{0.2}Zn_{0.8}O$ upper waveguide layer. The stack was then covered with a 50-nm-thick $Mg_{0.3}Zn_{0.7}O$ upper cladding layer, and capped with 150-nm Si_3N_4 for the grating. The active region consists of ten 3-nm-thick ZnO QWs with 7-nm-thick $Mg_{0.2}Zn_{0.8}O$ barrier layers in between. Similar waveguide simulations as in the sample with thin film active region together with a grating depth of 100 nm resulted in a simulated coupling strength of 550 cm^{-1}. Owing to the QW confinement shift, the emission wavelength of this sample was 360 nm, considerably shorter than that of the thin film device. However, the smaller effective index of this Mg-containing waveguide nevertheless resulted in a longer grating period of 276 nm.

Fig. 8 shows the far-field distribution of the DFB laser as a projection on a white sheet of paper and under different pump intensities. The rectangular spot depicts the direct reflection of the pump beam while the narrow slightly curved line is the surface emission (diffraction) of the ZnO multi-QW laser. While the pump beam is still clearly visible at the lowest intensity level, the ZnO laser beam fades away completely as soon as the threshold condition is no longer fulfilled. Note that the emission angle can be described by the standard grating formula taking into account the refractive index of the laser material.

Fig. 9 shows the light output versus pump intensity curves at different temperatures ranging from 11 up to

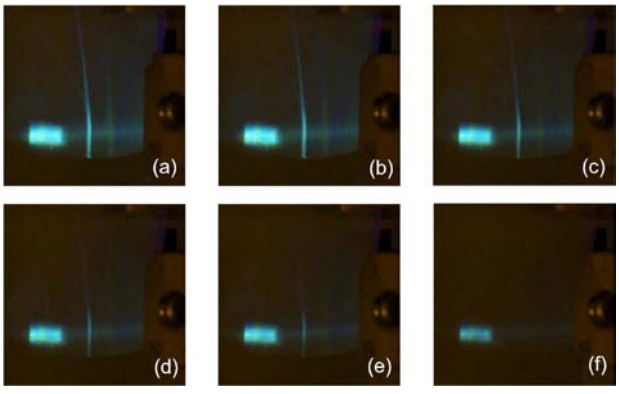

Fig. 8. ***Far-field distribution of a ZnO-based multi-QW DFB laser at different pump intensities [(a)–(f): 1.2, 1.0, 0.8, 0.6, 0.4, and 0.2 MW/cm^2]. The picture at the lower right-hand side is taken below threshold.***

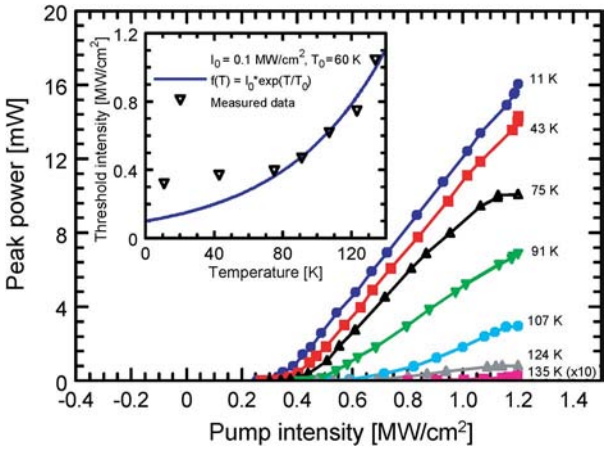

Fig. 9. ***Series of light output versus pump intensity curves for temperatures between 11 and 135 K. The inset shows the threshold intensity as a function of temperature. From these data, a characteristic temperature of $T_0 = 60$ K can be inferred.***

135 K. As expected, there is a linear relation between the two quantities above threshold. Although this particular device suffered from a relatively large mismatch between the Bragg reflection and the gain peak, a threshold intensity as low as 330 kW/cm^2 was achieved at 11 K. With a better match of the grating period, a substantial improvement to similar values as in the thin film device can be expected. The maximum peak output power reached 16 mW at low temperatures and a remarkably small linewidth of 1.5 Å was observed. All these characteristics indicate a high quality of the epitaxial material and a textbook behavior of the lasing properties; therefore, a promising performance for future ZnO laser experiments can be anticipated.

As an epilogue, it should again be mentioned that unavailability of reliable *p*-type conductivity prevents ZnO from competing with GaN for optoelectronic applications to a first extent. There are of course continuing developments in the GaN industry to satisfy the increasing demands for larger data storage capacity by developing short wavelength emitters of high efficiency, such as high-coherence and low-threshold UV/violet lasers. ZnO-based low-threshold or nearly thresholdless lasers, especially those based on polariton lasing in ZnO [28], will also have applications in ever increasing telecommunications and optical storage, in addition to being possible strong light pump sources for white light generation. Therefore, this too underlines the need to develop reliable *p*-type ZnO that will allow demonstration of high-efficiency ZnO light sources.

C. Transparent Conducting Oxides and TFTs

Although Si has shown its supremacy in the field of TFT technology with amorphous Si (*a*-Si) and polycrystalline-Si (poly-Si), an interest is developing for the optically transparent analog, the transparent thin film transistor (TTFT) technology [36]. Unlike conventional FET or TFT structures, TTFTs require all of the device components (channel, gate, electrodes, and substrate) to be transparent. Such invisible TTFTs can be used in wide range of commercial and military applications where transparency is required. The interest is in part because it is expected that the characteristics of TTFT will not degrade on exposure to visible light due to the wide bandgap of its active channel layer, whereas the characteristics of amorphous or poly-Si TFT degrade. Therefore, measures would not be required in this case to shield the active channel layer from visible light, unlike the commercial amorphous silicon transistors in which visible light generates excess carriers, and therefore, must be shielded. Also it should be noted that such invisible TFTs using ZnO as an active channel achieve much higher field effect mobilities than amorphous silicon transistors (0.5 cm^2/V-s), the major material of today's FET technology. Besides, high-quality crystalline ZnO films can be grown at relatively low deposition temperatures on various substrates including amorphous glasses.

Before delving into the discussion of transistor structures, a brief review of the transparent oxides based on ZnO in their own merits is warranted. In most optoelectronic devices such as flat panel displays, LEDs, and solar cells, it is essential to use a transparent electrode such as a thin film transparent conducting oxide (TCO). Although tin-doped ITO thin films deposited by magnetron sputtering are widely used today for most transparent electrode applications, there are many reports on other TCO semiconductors such as aluminum-doped zinc oxide (AZO), gallium-doped zinc oxide (GZO), indium-doped zinc oxide (IZO), tin-doped zinc oxide (TZO) in large part due to the expected worldwide shortage of In. The growing demand for ITO thin-film transparent electrodes is the impetus for looking at alternative TCO materials since a stable supply of ITO may be difficult to achieve for the expanding market because of the cost and, as mentioned, limited amount of indium available. ZnO-based TCOs have attracted significant attention due to their good conductivity, high optical transparency (in the 90% range), excellent surface smoothness, low deposition temperature, good etchability for patterning, and good reproducibility [37]–[39]. Candidates for transparent amorphous oxides having large electron mobilities must be constituted of heavy post-transition metal cations with an electronic configuration $(n-1)d^{10}ns^0$, where $n \geq 5$ [40]. Oxide semiconductor XZO films, where X = Al, Ga, In, Sn, are prepared from a target made of homogeneous $Al_2O_3(ZnO)_n$, $Ga_2O_3(ZnO)_n$, $In_2O_3(ZnO)_n$, or $SnO_2(ZnO)_n$ compounds. Although various dopants have been used to achieve ZnO TCO films, low resistivity (below $2 \times 10^{-4}\ \Omega \cdot$ cm) and high carrier concentration (above 10^{21} cm^{-3}) have only been obtained in AZO and GZO films, as can be seen from Table 1 [41]. For example, resistivities as low as $0.85 \times 10^{-4}\ \Omega$-cm and $0.81 \times 10^{-4}\ \Omega$-cm have been obtained for ZnO : Al [42] and ZnO : Ga [43] thin films grown by pulsed laser

Table 1 Minimum Resistivity and Maximum Carrier Concentration Obtained for ZnO Films Doped With Various Impurities. (After Minami [41].)

Dopant	Dopant content (Wt %)	Resistivity, $\times 10^{-4}$ Ω-cm	Carrier concentration, $\times 10^{20}$ cm^{-3}
Al_2O_3	1-2	0.85	15.4
Ga_2O_3	2-7	1.2	14.5
B_2O_3	2	2.0	5.4
Sc_2O_3	2	3.1	6.7
SiO_2	6	4.8	8.8
V_2O_5	0.5-3	5.0	4.9
F	0.5	4.0	5.0
Undoped	0	4.5	2.0

deposition, comparable to values obtained for ITO (e.g., 0.72×10^{-4} Ω-cm [44]). In general, the electrical properties of the TCO films strongly depend on the deposition methods and conditions. AZO and GZO films with resistivities on the order of 10^{-5} Ω-cm have been achieved by PLD, but preparing films on large substrates with high deposition rates is still challenging.

A typical schematic of a ZnO-based bottom-gate-type TTFT structure reported to have an optical transmission (including substrate) of ~75% for visible light is shown in Fig. 10 [45]. A glass substrate was blanket coated with a 200-nm-thick layer of sputtered ITO to serve as the gate and a 220-nm-thick layer of aluminum–titanium oxide (ATO) deposited by atomic layer deposition to serve as the gate insulator. After deposition of the ZnO layer by ion beam sputtering, a rapid thermal anneal, typically at 600 °C–800 °C in O_2, was employed to increase the ZnO channel resistivity in order to improve the electrical quality of the ATO/ZnO interface, and to enhance the crystallinity of the ZnO layer. Fig. 11 displays direct current (dc) electrical characteristics involving the drain current I_D, gate current I_G, gate voltage V_{GS}, and the drain voltage V_{DS}, for a ZnO channel TTFT having a channel length and width-to-length ratio of 1500 μm and 10 : 1, respectively. These curves indicate an *n*-channel, enhancement-mode TFT operation with excellent drain current saturation and a maximum drain current on-to-off ratio of $\sim10^7$. The effective channel mobility and the turn on gate voltage were found to be 0.35–0.45 cm^2/V-s and −12 V, respectively.

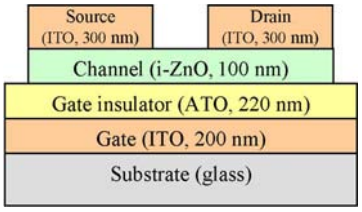

Fig. 10. ***The schematic of a typical ZnO channel enhancement mode TTFT structure. (After Hoffman et al. [45].)***

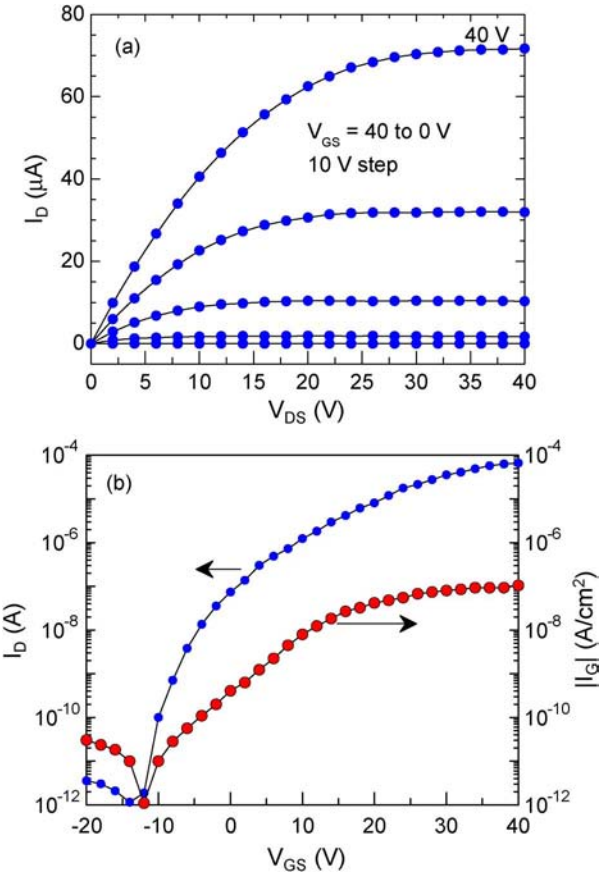

Fig. 11. ***Electrical characteristics of a ZnO channel TTFT: (a) drain current—drain voltage (I_D–V_{DS}) characteristics with the gate voltage V_{GS} from 0 to 40 V in 10-V increments; (b) transfer characteristics and gate leakage current for V_{DS} = 10 V. (After Hoffman et al. [45].)***

Song *et al.* [38] reported on TTFTs using amorphous ZnO : In (IZO) for the active channel layer and gate–source–drain electrodes fabricated by RF magnetron sputtering on glass substrates at room temperature while amorphous AlO_x served as the gate dielectric. The devices exhibited low threshold voltages of 1.1 V, on/off ratios of $\sim10^6$, saturation currents of 1.41 μA at 5 V, and optical transmittance of 80% (including the substrate) in the visible range. Nomura *et al.* [46] proposed a novel semiconducting material, amorphous oxide semiconductor In–Ga–Zn–O (*a*-IGZO), for the active channel in TTFTs. They deposited *a*-IGZO on polyethylene terephthalate (PET) at room temperature that exhibited a Hall effect mobility above 10 cm^2 V^{-1} s^{-1}. TTFTs fabricated on such PET sheets showed saturation mobilities of 6–9 cm^2 V^{-1} s^{-1}, and device characteristics were stable during repetitive bending of the TTFT sheet. The transfer characteristics showed a low off-current, of the order of 10^{-7} A, and a $\sim10^3$ on-to-off current ratio. Studies on the effect of bending on the TTFT characteristics showed that the performance of the TTFT after repetitive bending remained largely unaffected. Only a slight decrease in the saturation

current was observed. The TTFT was stable at temperatures up to 120 °C, but inoperative at higher temperatures, probably owing to the softening of the PET substrate.

Another key issue for ZnO TFTs is the selection of the gate insulator. Among the various gate dielectric materials tested, such as SiO_2, HfO_2, (Pb,Zr)TiO_3, ZnMgO, and Y_2O_3, high dielectric constant $Bi_{1.5}Zn_{1.0}Nb_{1.5}O_7$ (BZN) has been shown to result in very low operation voltages (< 4 V) in TTFTs with ZnO serving as the electron channel [47]. At an operating voltage of 4 V the devices exhibited a field effect mobility (drift mobility) and a current on/off ratio of 0.024 cm^2/V-s and 2×10^4, respectively, and the threshold voltage was 2 V. High optical transparency (> 80% for wavelengths above 400 nm), low-temperature processing, and low operation voltage of ZnO-based TFTs with integrated BZN dielectric are promising for transparent device technology.

Lowering the carrier concentration in a TFT channel is crucial for reducing the leakage current. This can be achieved by compensating the *n*-type carriers by acceptor doping. High-performance thin TTFTs with nitrogen-doped ZnO as the channel grown by atomic layer deposition on glass substrates have been demonstrated by Lim *et al.* [48]. The entire TFT fabrication process was carried out below 150 °C including the Al_2O_3 gate insulator deposition before the ZnO channel growth. By nitrogen doping, the electron concentration in ZnO was lowered to 6×10^{14} cm^{-3}. Consequently, the enhancement-mode TFT devices (40-μm channel width, 20-μm channel length) so produced exhibited off-currents as low as 2 pA, with a threshold (turn-on) voltage of 4.7 V, an on-to-off drain current ratio of 9.5×10^7, and a saturation mobility of 6.7 cm^2/V-s at 35-V drain bias. The devices with undoped ALD-grown ZnO channels did not show any pinch-off and depletion as the electron concentrations in the channel were up to 5×10^{19} cm^{-3}.

Enhancement-mode MgZnO-based field-effect transistors utilizing HfO_2 as the gate dielectric and ITO-coated glass substrates have also been reported [49]. A polycrystalline ZnO channel doped with Mg (10%) and P (2%, assuming that it serves as *p*-type compensating center) was used to decrease the electron carrier concentration. Mg doping increases the bandgap, and therefore, increases the activation energy for defect-related donors, helping the compensation of *n*-type carriers together with P doping. In these devices, an on/off ratio of 10^3 and channel mobility on the order of 5 cm^2/V-s were obtained. Another report [50] compared ZnO thin film metal–semiconductor field effect transistors (MESFETs) and metal–oxide–semiconductor (MOS) FETs with either P-doped (2%) or undoped ZnO channels and gate lengths as small as 1.5 μm. Growth of a $\sim$ 0.8–0.9-μm-thick ZnO buffer on sapphire or glass substrates was deemed necessary prior to depositing the active layers in order to reduce the gate leakage current. As would be expected due to the relatively low barrier height of metals on *n*-type ZnO (0.6–0.8 eV), the MOS structure with 50-nm-thick (Ce,Tb) $MgAl_{11}O_{19}$ gate dielectric showed an order of magnitude lower gate leakage current than the MESFET. The MOS gate structures using P-doped ZnO channels showed good depletion mode conductance modulation with a field-effect mobility of 5.32 cm^2/V-s, as compared to the very poor modulation by the metal structures.

Transparent nature of ZnO, potential achievement of low-cost polycrystalline ZnO, and fabrication technologies that are amenable to TFT production appear to suggest that ZnO may find a niche application in transparent thin film technologies with added features over the Si-based varieties.

III. PIEZOELECTRIC DEVICES

Due to its moderately high (very high for a semiconductor) electromechanical coupling coefficients, ZnO has been successfully used in thin film piezoelectric devices such as bulk acoustic wave and SAW resonators, filters, sensors, and microelectromechanical systems (MEMS), the most common application being the SAW filter, which has been an important component in mass consumer items such as TV filters and wireless communications systems. Successful development of sputtering of high-quality ZnO thin films on Si has been a breakthrough in the SAW device field as it allowed integration of ultrasonics with Si electronics for the first time, liberating device design from bulk piezoelectric substrates. For implementing acoustic-wave devices piezoelectric ZnO thin films grown on nonpiezoelectric substrates having high acoustic velocity and low propagation loss (diamond, sapphire), weakly piezoelectric materials such as quartz, amorphous substrates such as glass, and other semiconductors (Si, GaAs, InP, etc.) have been used.

SAW devices have been implemented with ZnO and $Mg_xZn_{1-x}O$ thin films grown on various substrates such as Si, GaAs, quartz, sapphire, SiC, diamond, GaN, and AlN [51], [52]. Fig. 12 shows the S_{21} scattering parameter (ratio of the transmitted signal amplitude to the incident signal amplitude) from a 10-μm wavelength [periodicity of the interdigitated transducer (IDT)] SAW device fabricated on a 1.5-μm-thick *a*-plane ZnO film grown on *r*-plane sapphire [53]. The central frequency is at $\sim$420 MHz (Rayleigh wave), which gives a sound velocity of 4200 m/s using $\lambda_0 = 10$ μm. A large effective electromechanical coupling coefficient K^2_{eff} of 6% was obtained. To reduce the conductivity and achieve piezoelectricity, the as-grown *n*-type ZnO films were compensated by Li doping during MOCVD growth.

To explore higher frequency capability, ZnO thin films have been prepared on high acoustic velocity materials such as SiC and AlN. SAW devices fabricated using 400-nm-thick ZnO thin films deposited on commercial SiC substrates have shown generalized SAW modes with acoustic velocities of 7000 m/s and pseudo-SAW modes with acoustic velocities of

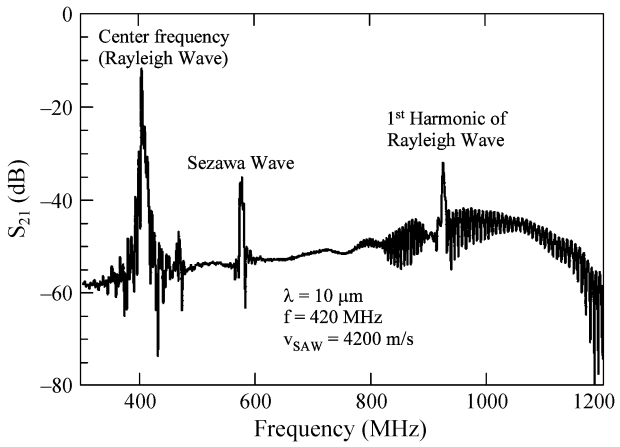

Fig. 12. ***Frequency response of a 10-μm wavelength SAW device on a 1.5-μm-thick ZnO film. (After Gorla et al. [53].)***

12 500 m/s [54]. ZnO thin films deposited on diamond, which has the highest acoustic velocities among all materials, have shown to exhibit SAW velocities as large as 11 600 m/s with coupling coefficients up to 1.1% [55]. Using 0.65-μm-wide electrode devices with a center frequency of 10 GHz, a coupling coefficient of 1.5% was also demonstrated for the fifth harmonic of the second Sezawa mode [56]. All the aforementioned results show that ZnO thin films on various substrates can be successfully implemented as efficient SAW devices. Even though piezoelectric materials such as $LiNbO_3$ and $LiTaO_3$ have larger electromechanical coupling coefficients, as high as 38% and 14%, respectively, ZnO is promising for applications that require electroacoustic modulation and monolithic integration with other semiconductor technologies.

ZnO-based SAW devices have been used for UV photodetection [57] and for gas [58] and biochemical [59] sensing. The SAW UV photodetector is based on the acoustoelectric interaction. The photogenerated carriers increase the conductivity in the material which in turn increases the attenuation and decreases the SAW velocity, and therefore, the SAW frequency. SAW UV detectors with ZnO piezoelectric layers (highly compensated by Li doping with a resistivity above 10^7 Ω-cm) have also been demonstrated on *r*-sapphire using a thin $Mg_{0.2}Zn_{0.8}O$ buffer layer in between for isolation and as a diffusion barrier for Li [57]. The IDTs were placed on the piezoelectric layer with the ZnO UV absorbing layer in between the transmitter and receiver IDTs. A frequency shift up to 11 MHz and an insertion loss increase of ~23 dB were observed in the central Sezawa mode frequency (711 MHz) when the device was illuminated with 365-nm light of intensity 2.32 mW/cm^2. The corresponding maximum phase shift was measured at 365 nm as 107°. ZnO SAW UV detectors with such performance were proposed for use as passive zero-power remote wireless sensors [57].

IV. SENSORS AND SOLAR CELLS BASED ON ZnO NANOSTRUCTURES

ZnO nanorod/nanowire FET sensors may create opportunities for highly sensitive and selective real-time detection of a wide variety of gas molecules and biomolecules. The principle of gas sensor operation depends on the nature of gas molecules and is based on the modification of nanowire FET channel conductivity. Oxygen vacancies in ZnO function as *n*-type donors on oxide surfaces and are electrically and chemically active. Upon adsorption of charge accepting gas molecules, for example, NO_2 and O_2, electrons are depleted from the conduction band resulting in a reduced conductivity of the *n*-type oxide. On the other hand, molecules that chemically react with surface oxygen (for example, CO and H_2) interact with surface adsorbed oxygen on ZnO and remove it leading to an increase in conductivity. ZnO exhibits strong adsorption of molecules on the surface, which affects the electrical characteristics of ZnO-based devices, dependent on surface-mediated phenomena. Thanks to the large surface-to-volume ratio of the nanostructures, the detection sensitivity of FET biosensors may be increased to a single-molecular detection level by measuring the small conductance changes caused by binding of biomolecular species on a nanorod conduction channel.

A. Gas Sensors

There is a strong interest in the development of lightweight gas sensors capable of parts per million (ppm) range sensitivity and extended operation at low-power levels. All experimental results demonstrate that ZnO nanowires, owing to the large surface area, have a potential for detecting NO_2 [60], NH_3 [61], NH_4 [62], CO [62], H_2 [63], H_2O [64], O_3 [65], H_2S [66], and C_2H_5OH [67]. Detection of gas molecules is usually achieved by measuring the resistivity change of either the nanocrystalline ZnO films or the nanowire channel of an FET.

Cho *et al.* [60] reported a 1.8 fold decrease in resistance of well-dispersed ZnO nanorods at 1-ppm NO_2, while there was no significant change in resistance at 50-ppm CO. Sputtered nano-crystallite Cu-doped ZnO films of columnar structure with average grain size of 5 nm exhibited very high sensitivity (2.7–20 ppm) to CO at 350 °C [62]. A substantial change in resistance of the ZnO films was also observed at a low operating temperature of 150 °C when the sensor was exposed to 6-ppm CO. The sensitivity for room temperature detection of hydrogen by ZnO nanorods was shown to be greatly enhanced by sputter-depositing clusters of Pd on the surface [63]. An increase in the resistivity by a factor of 5 was observed upon exposure to hydrogen concentrations of 10–500 ppm compared to that without Pd. Pd-coated ZnO nanorods showed sensitivities lower than 10 ppm, with 95% recovery of the initial conductance after 20 s.

ZnO nanorods are also promising candidates for detecting extremely low concentrations of H_2S. High

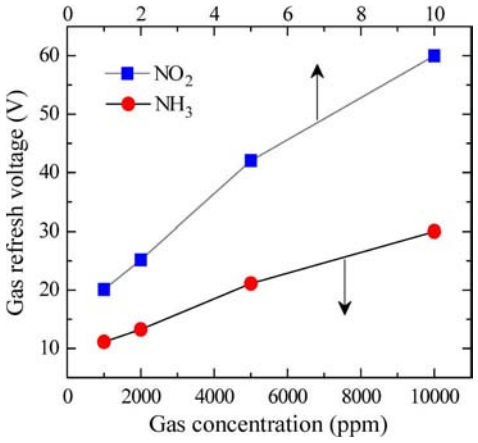

Fig. 13. *Gate refresh voltages of a ZnO nanowire FET for NH_3 and NO_2 gas molecules as a function of gas concentration. (After Fan and Lu [68].)*

response and good selectivity of ZnO nanorods to low concentrations of H_2S was observed by Wang *et al.* [66]. The ratio of the electrical resistance in air to that in 0.05-ppm H_2S was measured to be 1.7 at room temperature. One of the most important parameters of gas sensors is their selectivity. The selectivity is achieved by applying different voltages to the gate of a nanowire FET or by performing measurements at different temperatures since different gas molecules have different activation energies. Fig. 13 shows an example of such selectivity for NH_3 and NO_2 gas molecules, where the refresh (erase) voltages, negative gate voltages required for electrical desorption of adsorbed gas molecules, for the two gas molecules are significantly different making it possible to distinguish different gas species [68].

B. Biosensors

The potential of ZnO nanostructures as nanosized biosensors has also been explored for detecting different biological molecules. Development of 1-D ZnO nanostructures as biosensors is in the embryonic stage and only a limited number of reports are available [69]–[74]. The 1-D ZnO biosensors have advantages such as stability in air, nontoxicity, chemical stability, electrochemical activity, ease of synthesis, and bio-safe characteristics. As in the case of gas sensors, the principle of operation is that the conductance of ZnO nanorod FETs drastically changes when biomolecules are adsorbed.

The key factor in most biological processes is the need for a small change of the pH concentration created by the release of H^+ ions during biochemical reactions. Therefore, determination of pH is a prerequisite for many processes. The sensing mechanism for pH is the polarization-induced bound surface charge by interaction with the polar molecules in the liquids. Application of ZnO nanorods as pH sensors for intracellular chemical sensing is under development and a room temperature sensitivity (change in surface potential) as high as ~59 mV per decade change in the pH value has been reported [74].

C. Solar Cells

Solar cells represent a very promising renewable energy technology because they provide clean (beyond manufacturing) and renewable energy reducing our dependence on fossil oil and our impact on the environment. Dye-sensitized solar cells (DSSCs), using inorganic semiconductors, are being studied for very efficient, inexpensive, large-scale solar energy conversion. DSSCs have been explored as possible substitutes for conventional silicon cells, but they suffer from possible dye agglomeration or electrolyte leakage [75]–[79].

During its traversal to the photoelectrode, an electron in a polycrystalline solar cell usually crosses about 10^3 to 10^6 nanoparticles, and disorder structure of the nanoparticle film leads to enhanced scattering of free electrons, thus reducing the electron mobility and increasing detrimental electron recombination rate. Replacement of the nanoparticle film with an array of oriented single-crystalline nanorods would result in the rapid collection of carriers generated throughout the device as the nanorods provide a direct path from the point of photogeneration to the conducting substrate, thus effectively reducing the electron recombination losses. Fig. 14 shows a typical DSSC structure, which has three main components: 1) a thick (~10 μm) film of wide bandgap semiconductor nanostructures (TiO_2, SnO_2, or ZnO), 2) a monolayer of organic dye molecules absorbed onto the semiconductor nanostructures, and 3) a liquid electrolyte containing the redox (reduction-oxidation reaction) couple I^-/I_3^- that penetrates in between the dye-coated nanostructures. Electron transport in the single crystalline rod is expected to be several orders of magnitude faster than that in a random polycrystalline network. However, increased surface area by nanorods, as compared to thin films, also increases the surface recombination causing reduction in efficiency.

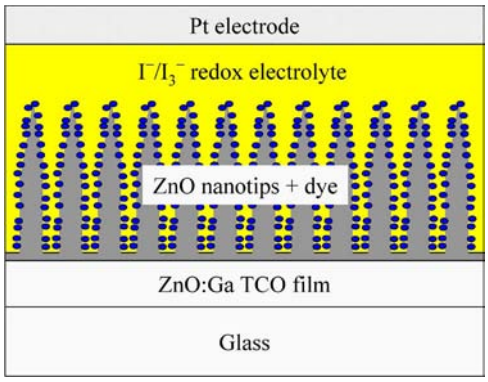

Fig. 14. *A schematic of a nanotip ZnO-based DSSCs. (Courtesy of Y. Lu.)*

V. CONCLUDING REMARKS

ZnO offers some potential in providing electronic, photonic, and spin-based devices, and encouraging progress has been made in the research phase. Despite this progress, there is still a number of important issues that are in need of further investigation before this material can be transitioned to commercial use for the stated applications. The task is made more difficult by the highly successful GaN which competes for similar applications. However, there are some niche applications of ZnO which are not addressed by GaN which if explored fully might pave the way for ZnO. TTFT, ZnO-based transparent oxides, laser structures exploiting the large exciton binding energy of ZnO are among these applications.

In the case of TTFTs, the critical issues are the mobility in noncrystalline or polycrystalline ZnO, and the choice of gate oxide, substrate, and the methods to deal with high electron concentrations encountered in ZnO channel layers. For electrical characteristics, the on-to-off ratio as well as the transconductance is important to home in on.

ZnO also lends itself to applications in sensing, in part due to ease with which ZnO can be produced in the form of nanostructures. There is still much to be understood in terms of the mechanism of ZnO gas sensors and biosensors. Although a number of ZnO sensors have been reported on detecting different gas molecules and biomolecules, the selectivity (not unique to ZnO) remains to be the main issue since identification of the nature of the absorbed molecules is very important. Although several approaches have been proposed, which employ different activation energies of different gas molecules, this field is still in a state of infancy and much more effort needs to be expended to pave the way for improved selectivity of ZnO sensors and increase the lifetime of the devices.

Regarding solar sells, which received some attention although the competition is very stiff, further studies are required to improve the current density and efficiency. This could be achieved by application of various electrolytes [80] and doping the ZnO films to improve its conductivity. There is also the control of the properties of individual building blocks which at this point is inadequate and device-to-device reproducibility is low.

As for the nanostructures, ZnO nanostructures (nanowires, nanorods, etc.) provide a path to a new generation of devices, but a deliberate effort has to be expended for ZnO nanostructures to be taken seriously for large-scale device applications, and to achieving high device density with accessibility to individual nanodevices. Reliable methods for assembling and integrating building blocks into circuits need to be developed.

Finally, ZnO as a semiconductor is facing a very stiff competition from GaN which is much more mature in terms of devices (also has acceptable *p*-type dopant unlike the case in ZnO). Lack of a credible *p*-type doping hampers widespread optical emitters in ZnO. Furthermore, highly ionic nature of ZnO with large electron phonon coupling and low thermal conductivity does not bode well for ZnO-based electronic devices. Nanostructures seem a little easier to produce with ZnO, but it remains to be seen whether nanostructures in general as hyped would really make inroads in the area of devices. ■

REFERENCES

[1] P. C. Chang, Z. Fan, C. J. Chien, D. Stichtenoth, C. Ronning, and J. G. Lu, "High-performance ZnO nanowire field effect transistors," *Appl. Phys. Lett.*, vol. 89, pp. 133113-1–133113-3, Sep. 2006.

[2] W. I. Park, J. S. Kim, G.-C. Yi, M. H. Bae, and H.-J. Le, "Fabrication and electrical characteristics of high-performance ZnO nanorod field-effect transistors," *Appl. Phys. Lett.*, vol. 85, pp. 5052–5054, Nov. 2004.

[3] Z. Fan and J. G. Lu, "Electrical properties of ZnO nanowire field effect transistors characterized with scanning probes," *Appl. Phys. Lett.*, vol. 86, pp. 032111-1–032111-3, Jan. 2005.

[4] P. Yang, H. Yan, S. Mao, R. Russo, J. Johnson, R. Saykally, N. Morris, J. Pham, R. He, and H.-J. Choi, "Controlled growth of ZnO nanowires and their optical properties," *Adv. Funct. Mater.*, vol. 12, pp. 323–331, May 2002.

[5] Q. Wan, Q. H. Li, Y. J. Chen, T. H. Wang, X. L. He, J. P. Li, and C. L. Lin, "Fabrication and ethanol sensing characteristics of ZnO nanowire gas sensors," *Appl. Phys. Lett.*, vol. 84, pp. 3654–3656, Apr. 2004.

[6] C. H. Liu, J. A. Zapien, Y. Yao, X. M. Meng, C. S. Lee, S. S. Fan, Y. Lifshitz, and S. T. Lee, "High-density, ordered ultraviolet light-emitting ZnO nanowire arrays," *Adv. Mater.*, vol. 15, pp. 838–841, May 2003.

[7] H. Kind, H. Yan, B. Messer, M. Law, and P. Yang, "Nanowire ultraviolet photodetectors and optical switches," *Adv. Mater.*, vol. 14, pp. 158–160, Jan. 2002.

[8] Ü. Özgür, Y. I. Alivov, C. Liu, A. Teke, M. Reshchikov, S. Doğan, V. Avrutin, S.-J. Cho, and H. Morkoç, "A comprehensive review of ZnO materials and devices," *J. Appl. Phys.*, vol. 98, pp. 041301-1–041301-103, Aug. 2005.

[9] D. C. Look and B. Claflin, "P-type doping and devices based on ZnO," *Phys. Stat Sol. B*, vol. 241, pp. 624–630, Feb. 2004.

[10] C. Coskun, D. C. Look, G. C. Farlow, and J. R. Sizelove, "Radiation hardness of ZnO at low temperatures," *Semicond. Sci. Technol.*, vol. 19, pp. 752–754, Jun. 2004.

[11] D.-K. Hwang, M.-S. Oh, J.-H. Lim, Y.-S. Choi, and S.-J. Park, "ZnO-based light emitting metal-insulator-semiconductor diodes," *Appl. Pys. Lett.*, vol. 91, pp. 121113-1–121113-3, Sep. 2007.

[12] M. Nakano, T. Makino, A. Tsukazaki, K. Ueno, A. Ohtomo, T. Fukumura, H. Yuji, S. Akasaka, K. Tamura, K. Nakahara, T. Tanabe, A. Kamisawa, and M. Kawasaki, "Transparent polymer Schottky contact for a high performance visible-blind ultraviolet photodiode based on ZnO," *Appl. Phys. Lett.*, vol. 93, pp. 123309-1–1233039-3, Sep. 2008.

[13] I. T. Drapak, "Visible luminescence of a ZnO–Cu_2O heterojunction," *Semiconductors*, vol. 2, pp. 624–625, 1968.

[14] Y. I. Alivov, E. V. Kalinina, A. E. Cherenkov, D. C. Look, B. M. Ataev, A. K. Omaev, M. V. Chukichev, and D. M. Bagnall, "Fabrication and characterization of n-ZnO/p-AlGaN heterojunction light-emitting diodes on 6H-SiC substrates," *Appl. Phys. Lett.*, vol. 83, pp. 4719–4721, Dec. 2003.

[15] A. Osinsky, J. W. Dong, M. Z. Kauser, B. Hertog, A. M. Dabiran, P. P. Chow, S. J. Pearton, O. Lopatiuk, and L. Chernyak, "MgZnO/AlGaN heterostructure light emitting diodes," *Appl. Phys. Lett.*, vol. 85, pp. 4272–4274, Nov. 2004.

[16] A. Tsukazaki, A. Ohtomo, T. Onuma, M. Ohtani, T. Makino, M. Sumiya, K. Ohtani, S. F. Chichibu, S. Fuke, Y. Segawa, H. Ohno, H. Koinuma, and M. Kawasaki, "Repeated temperature modulation epitaxy for p-type doping and light-emitting diode based on ZnO," *Nature Mater.*, vol. 4, pp. 42–46, Jan. 2005.

[17] A. Tsukazaki, M. Kubota, A. Ohtomo, T. Onuma, K. Ohtani, H. Ohno, S. F. Chichibu, and M. Kawasaki, "Blue light-emitting diode based on ZnO," *Jpn. J. Appl. Phys.*, vol. 44, pp. L643–L645, May 2005.

[18] V. Avrutin, D. Silversmith, and H. Morkoç, "Doping asymmetry problem in ZnO: Current status and outlook, *IEEE Proc.*, vol. 98, no. 7, Jul. 2010.

[19] O. Bierwagen, T. Ive, C. G. Van de Walle, and J. S. Speck, "Causes of incorrect carrier-type identification in van der Pauw-Hall measurements," *Appl. Phys. Lett.*, vol. 93, pp. 242108-1–242108-3, Dec. 2008.

[20] J. L. Lyons, A. Janotti, and C. G. Van de Walle, "Why nitrogen cannot lead to p-type conductivity in ZnO," *Appl. Phys. Lett.*, vol. 95, pp. 252105-1–252105-3, Dec. 2009.

[21] J.-H. Lim, C.-K. Kang, K.-K. Kim, I.-K. Park, D.-K. Hwang, and S.-J. Park, "UV electroluminescence emission from ZnO light-emitting diodes grown by high-temperature radiofrequency sputtering," *Adv. Mater.*, vol. 18, pp. 2720–2724, Sep. 2006.

[22] Y. R. Ryu, T. S. Lee, J. A. Lubguban, H. W. White, B. J. Kim, Y. S. Park, and C. J. Youn, "Next generation of oxide photonic devices: ZnO-based ultraviolet light emitting diodes," *Appl. Phys. Lett.*, vol. 88, pp. 241108-1–241108-3, Jun. 2006.

[23] Y. R. Ryu, J. A. Lubguban, T. S. Lee, H. W. White, T. S. Jeong, C. J. Youn, and B. J. Kim, "Excitonic ultraviolet lasing in ZnO-based light emitting devices," *Appl. Phys. Lett.*, vol. 90, pp. 131115-1–131115-3, Mar. 2007.

[24] J. Zhong, H. Chen, G. Saraf, Y. Lu, C. K. Choi, and J. J. Song, "Integrated ZnO nanotips on GaN light emitting diodes for enhanced emission efficiency," *Appl. Phys. Lett.*, vol. 90, pp. 203515-1–203515-3, May 2007.

[25] X. Wu, A. Yamilov, X. Liu, S. Li, V. P. Dravid, R. P. H. Chang, and H. Cao, "Ultraviolet photonic crystal laser," *Appl. Phys. Lett.*, vol. 85, pp. 3657–3659, Oct. 2004.

[26] M. Scharrer, A. Yamilov, X. Wu, H. Cao, and R. P. H. Chang, "Ultraviolet lasing in high-order bands of three dimensional; ZnO photonic crystals," *Appl. Phys. Lett.*, vol. 88, pp. 201103-1–201103-3, May 2006.

[27] H. Cao, Y. G. Zhao, S. T. Ho, E. W. Seeling, Q. H. Wang, and R. P. H. Chang, "Random laser action in semiconductor powder," *Phys. Rev. Lett.*, vol. 82, pp. 2278–2281, Mar. 1999.

[28] R. Shimada and H. Morkoç, "Wide bandgap semiconductor-based surface emitting lasers," *IEEE Proc.*, vol. 98, no. 7, Jul. 2010.

[29] G. A. Evans, D. P. Bour, N. W. Carlson, J. M. Hammer, M. Lurie, J. K. Butler, S. L. Palfrey, R. Amantea, L. A. Carr, F. Z. Hawrylo, E. A. James, J. B. Kirk, S. K. Liew, and W. F. Reichert, "Coherent, monolithic two-dimensional strained InGaAs/AlGaAs quantum well laser arrays using grating surface emission," *Appl. Phys. Lett.*, vol. 55, no. 26, pp. 2721–2723, Dec. 1989.

[30] D. Hofstetter, M. Kneissl, D. P. Bour, C. Dunnrowicz, and R. L. Thornton, "Demonstration of an optically pumped InGaN/GaN-based MQW DFB laser using holographically defined 3rd order gratings," *Appl. Phys. Lett.*, vol. 73, no. 14, pp. 1928–1930, Oct. 1998.

[31] D. Hofstetter, R. L. Thornton, L. T. Romano, D. P. Bour, M. Kneissl, and R. M. Donaldson, "Room temperature pulsed operation of InGaN/GaN-based multi quantum well distributed feedback laser," *Appl. Phys. Lett.*, vol. 73, no. 15, pp. 2158–2160, Oct. 1998.

[32] M. Kneissl, D. P. Bour, C. G. Van de Walle, L. T. Romano, J. E. Northrup, R. M. Wood, M. Teepe, and N. M. Johnson, "Room-temperature continuous-wave operation of InGaN multiple-quantum-well laser diodes with an asymmetric waveguide structure," *Appl. Phys. Lett.*, vol. 75, no. 4, pp. 581–583, Jul. 1999.

[33] H. Kogelnik and C. V. Shank, "Coupled-wave theory of distributed feedback lasers," *J. Appl. Phys.*, vol. 43, no. 5, pp. 2327–2335, May 1972.

[34] D. Hofstetter, Y. C. Bonetti, A. H. El-Shaer, A. Bakin, A. Waag, R. Schmidt-Grund, M. Schubert, and M. Grundmann, "Demonstration of an ultraviolet ZnO-based optically pumped 3rd order distributed feedback laser," *Appl. Phys Lett.*, vol. 91, no. 11, pp. 111108-1–111108-3, Sep. 2007.

[35] D. Hofstetter, R. Theron, A.-H. El-Shaer, A. Bakin, and A. Waag, "Demonstration of a ZnO/MgZnO-based one-dimensional photonic crystal multi-quantum well laser," *Appl. Phys Lett.*, vol. 93, no. 10, pp. 101109-1–101109-3, Sep. 2008.

[36] R. Hoffman, "ZnO thin-film transistors," in *Zinc Oxide Bulk, Thin Films and Nanostructures: Processing, Properties and Applications*, C. Jagadish and S. J. Pearton, Eds. Amsterdam, The Netherlands: Elsevier, 2006, pp. 415–442.

[37] N. L. Dehuff, E. S. Kettenring, D. Hong, H. Q. Chiang, J. F. Wager, R. L. Hoffman, C.-H. Park, and D. A. Keszler, "Transparent thin-film transistors with zinc indium oxide channel layer," *J. Appl. Phys.*, vol. 97, pp. 064505-1–064505-5, Mar. 2005.

[38] J.-I. Song, J.-S. Park, H. Kim, Y.-W. Heo, J.-H. Lee, J.-J. Kim, and B. D. Choi, "Transparent amorphous indium zinc oxide thin-film transistors fabricated at room temperature," *Appl. Phys. Lett.*, vol. 90, pp. 022106-1–022106-3, Jan. 2007.

[39] N. Ito, Y. Sato, P. K. Song, A. Kaijio, K. Inoue, and Y. Shigesato, "Electrical and optical properties of amorphous indium zinc oxide films," *Thin Solid Films*, vol. 496, pp. 99–103, Feb. 2006.

[40] H. Hosono, "Ionic amorphous oxide semiconductors: Material design, carrier transport, and device application," *J. Non-Crystalline Solids*, vol. 352, pp. 851–858, Jun. 2006.

[41] T. Minami, "Transparent conducting oxide semiconductors for transparent electrodes," *Semicond. Sci. Technol.*, vol. 20, pp. S35–S44, Apr. 2005.

[42] H. Agura, A. Suzuki, T. Matsushita, T. Aoki, and M. Okuda, "Low resistivity transparent conducting Al-doped ZnO films prepared by pulsed laser deposition," *Thin Solid Films*, vol. 445, pp. 263–267, Dec. 2003.

[43] S.-M. Park, T. Ikegami, and K. Ebihara, "Effects of substrate temperature on the properties of Ga-doped ZnO by pulsed laser deposition," *Thin Solid Films*, vol. 513, pp. 90–94, Aug. 2006.

[44] A. Suzuki, T. Matsushita, T. Aoki, and Y. Yoneyama, "Pulsed laser deposition of transparent conducting indium tin oxide films in magnetic field perpendicular to plume," *Jpn. J. Appl. Phys.*, vol. 40, pp. L401–L403, Apr. 2001.

[45] R. L. Hoffman, B. J. Norris, and J. F. Wager, "ZnO-based transparent thin-film transistors," *Appl. Phys. Lett.*, vol. 82, pp. 733–775, Feb. 2003.

[46] K. Nomura, H. Ohta, A. Takagi, T. Kamiya, M. Hirano, and H. Hosono, "Room-temperature fabrication of transparent flexible thin-film transistors using amorphous oxide semiconductors," *Nature*, vol. 432, no. 7016, pp. 488–492, Nov. 2004.

[47] I.-D. Kim, Y. W. Choi, and H. L. Tuller, "Low-voltage ZnO thin-film transistors with high- κ $Bi_{1.5}Zn_{1.0}Nb_{1.5}O_7$ gate insulator for transparent and flexible electronics," *Appl. Phys. Lett.*, vol. 87, pp. 043509-1–043509-3, Jul. 2005.

[48] S. J. Lim, S.-J. Kwon, H. Kim, and J.-S. Park, "High performance thin film transistor with low temperature atomic layer deposition nitrogen-doped ZnO," *Appl. Phys. Lett.*, vol. 91, 2007, 183517.

[49] Y. Kwon, Y. Li, Y. W. Heo, M. Jones, P. H. Holloway, D. P. Norton, Z. V. Park, and S. Li, "Enhancement-mode thin-film field-effect transistor using phosphorus-doped (Zn,Mg)O channel," *Appl. Phys. Lett.*, vol. 84, pp. 2685–2687, 2004.

[50] C. J. Kao, Y. W. Kwon, Y. W. Heo, D. P. Norton, S. J. Pearton, F. Ren, and G. C. Chi, "Comparison of ZnO metal-oxide-semiconductor field effect transistor and metal-semiconductor field effect transistor structures grown on sapphire by pulsed laser deposition," *J. Vac. Sci. Technol. B*, vol. 23, pp. 1024–1028, 2005.

[51] Y. Lu, N. W. Emanetoglu, and Y. Chen, "ZnO piezoelectric devices," in *Zinc Oxide Bulk, Thin Films and Nanostructures: Processing, Properties and Applications*, C. Jagadish and S. J. Pearton, Eds. Amsterdam, The Netherlands: Elsevier, 2006, pp. 443–489.

[52] N. W. Emanetoglu, S. Muthukumar, P. Wu, R. Wittstruck, Y. Chen, and Y. Lu, "$Mg_xZn_{1-x}O$: A new piezoelectric material," *IEEE Trans. Ultrason. Ferroelectr. Freq. Control*, vol. 50, no. 5, pp. 537–543, May 2003.

[53] C. R. Gorla, N. W. Emanetoglu, S. Liang, W. E. Mayo, Y. Lu, M. Wraback, and H. Shen, "Structural, optical, and surface acoustic wave properties of epitaxial ZnO films grown on (01–12) sapphire by metalorganic chemical vapor deposition," *J. Appl. Phys.*, vol. 85, pp. 2595–2602, 1999.

[54] I. S. Didenko, F. S. Hickernell, and N. F. Naumenko, "The experimental and theoretical characterization of the SAW propagation properties for zinc oxide films on silicon carbide," *IEEE Trans. Ultrason. Ferroelectr. Freq. Control*, vol. 47, no. 1, pp. 179–187, Jan. 2000.

[55] K. Higaki, H. Nakahata, H. Kitabayashi, S. Fujii, K. Tanabe, Y. Seki, and S. Shikata, "High frequency SAW filter on diamond," *IEEE MTT-S Digest*, vol. 2, pp. 829–832, 1997.

[56] H. Nakahata, A. Hachigo, K. Itakura, and S. Shikata, "Fabrication of high frequency SAW filters from 5 to 10 GHz using SiO_2/ZnO/diamond structure," in *Proc. IEEE Ultrasonic Symp.*, 2000, vol. 1–2, pp. 349–352.

[57] N. W. Emanetoglu, J. Zhu, Y. Chen, J. Zhong, Y. Chen, and Y. Lu, "Surface acoustic wave ultraviolet photodetectors using epitaxial ZnO multilayers grown on r-plane sapphire," *Appl. Phys. Lett.*, vol. 85, pp. 3702–3704, 2004.

[58] S. J. Ippolito, S. Kandasamy, K. Kalantar-Zadeh, W. Wlodarski, K. Galatsis, G. Kiriakidis, N. Katsarakis, and M. Suchea, "Highly sensitive layered ZnO/$LiNbO_3$ SAW device with InO_x selective layer for NO_2 and H_2 gas sensing," *Sens. Actuators B*, vol. 111–112, pp. 207–212, 2005.

[59] Z. Zhang, N. W. Emanetoglu, G. Saraf, Y. Chen, P. Wu, J. Zhong, Y. Lu, J. Chen, O. Mirochnitchenko, and M. Inouye, "DNA immobilization and SAW response in ZnO nanotips grown on $LiNbO_3$ substrates," *IEEE Trans. Ultrason. Ferroelectr. Freq. Control*, vol. 53, no. 4, pp. 786–792, Apr. 2006.

[60] P. S. Cho, K. W. Kim, and J. H. Lee, "NO2 sensing characteristics of ZnO nanorods prepared by hydrothermal method," *J. Electroceram.*, vol. 17, pp. 975–978, 2006.

[61] G. S. Devi, V. B. Subrahmanyam, S. C. Gadkari, and S. K. Gupta, "NH3 gas sensing properties of nanocrystalline ZnO based thick films," *Analytica Chimica Acta*, vol. 568, pp. 41–46, 2006.

[62] H. Gong, J. Q. Hu, J. H. Wang, C. H. Ong, and F. R. Zhu, "Nano-crystalline Cu-doped ZnO

thin film gas sensor for CO," *Sens. Actuators B, Chem.*, vol. 115, pp. 247–251, 2006.

[63] H. T. Wang, B. S. Kang, F. Ren, L. C. Tien, P. W. Sadik, D. P. Norton, S. J. Pearton, and J. Lin, "Hydrogen-selective sensing at room temperature with ZnO nanorods," *Appl. Phys. Lett.*, vol. 86, pp. 243503-1–243503-3, 2005.

[64] X. H. Wang, Y. F. Ding, J. Zhang, Z. Q. Zhu, S. Z. You, S. Q. Chen, and J. Z. Zhu, "Humidity sensitive properties of ZnO nanotetrapods investigated by a quartz crystal microbalance," *Sens. Actuators B, Chem.*, vol. 115, pp. 421–427, 2006.

[65] S. Christoulakis, M. Suchea, E. Koudoumas, M. Katharakis, N. Katsarakis, and G. Kiriakidis, "Thickness influence on surface morphology and ozone sensing properties of nanostructured ZnO transparent thin films grown by PLD," *Appl. Surface Sci.*, vol. 252, pp. 5351–5354, 2006.

[66] C. H. Wang, X. F. Chu, and M. W. Wu, "Detection of H_2S down to ppb levels at room temperature using sensors based on ZnO nanorods," *Sens. Actuators B, Chem.*, vol. 113, pp. 320–323, 2006.

[67] T. F. Xue, J. F. Hu, H. W. Qin, Y. Zhou, K. An, L. Zhang, T. Han, and Y. X. Li, "Sensing properties of the ZnO based composite oxide (Al,Sb)/ZnO to C_2H_5OH gas," *Rare Metal Mater. Eng.*, vol. 33, pp. 1006–1008, 2004.

[68] Z. Fan and J. G. Lu, "Gate-refreshable nanowire chemical sensors," *Appl. Phys. Lett.*, vol. 86, pp. 123510-1–123510-3, 2005.

[69] J. S. Kim, W. I. Park, C.-H. Lee, and G.-C. Yi, "ZnO nanorod biosensor for highly sensitive detection of specific protein binding," *J. Korean Phys. Soc.*, vol. 49, pp. 1635–1639, 2006.

[70] P. D. Batista and M. Mulato, "ZnO extended-gate field-effect transistors as pH sensors," *Appl. Phys. Lett.*, vol. 87, pp. 143508-1–143508-3, 2005.

[71] B. S. Kang, F. Ren, Y. W. Heo, L. C. Tien, D. P. Norton, and S. J. Pearton, "pH measurements with single ZnO nanorods integrated with a microchannel," *Appl. Phys. Lett.*, vol. 86, pp. 112105-1–112105-1, 2005.

[72] O. Dulub, B. Meyer, and U. Diebold, "Observation of the dynamical change in a water monolayer adsorbed on a ZnO surface," *Phys. Rev. Lett.*, vol. 95, pp. 136101-1–136101-4, 2005.

[73] S. M. Al-Hillia, M. Willander, A. Öst, and P. Strålfors, "ZnO nanorods as an intracellular sensor for pH measurements," *J. Appl. Phys.*, vol. 102, pp. 084304-1–084304-5, 2007.

[74] S. M. Al-Hilli, R. T. Al-Mofarji, and M. Willander, "Zinc oxide nanorod for intracellular pH sensing," *Appl. Phys. Lett.*, vol. 89, pp. 173119-1–173119-3, 2006.

[75] W. J. E. Beek, M. M. Wienk, and R. A. J. Janssen, "Efficient hybrid solar cell from zinc oxide nanoparticles and a conjugated polymer," *Adv. Mater.*, vol. 16, pp. 1009–1013, 2004.

[76] M. Law, L. Greene, J. C. Johnson, R. Saykally, and P. Yang, "Nanowire dye-sensitized solar cells," *Nature*, vol. 4, pp. 455–459, 2005.

[77] A. Du Pasquier, H. Chen, and Y. Lu, "Dye sensitized solar cells using well-aligned zinc oxide nanotip arrays," *Appl. Phys. Lett.*, vol. 89, pp. 253513-1–253513-3, 2006.

[78] J. B. Baxter and E. S. Aydil, "Nanowire-based dye-sensitized solar cells," *Appl. Phys. Lett.*, vol. 86, pp. 053114-1–053114-3, 2005.

[79] C. Y. Jiang, X. W. Sun, G. Q. Lo, D. L. Kwong, and J. X. Wang, "Improved dye-sensitized solar cells with a ZnO-nanoflower photoanode," *Appl. Phys. Lett.*, vol. 90, pp. 263501-1–263501-3, 2007.

[80] B. O'Regan and M. Grätzel, "A low-cost, high-efficiency solar cell based on dye-sensitized colloidal TiO_2 films," *Nature*, vol. 353, pp. 737–740, 1991.

ABOUT THE AUTHORS

Ümit Özgür (Member, IEEE) received the B.S. degree in electrical engineering and physics from Bogazici University, Istanbul, Turkey, in 1996, and the M.A. and Ph.D. degrees in physics from Duke University, Durham, NC, in 1999 and 2003, respectively.

He joined the Electrical and Computer Engineering Department, Virginia Commonwealth University, Richmond, in 2008, as an Assistant Professor. He is the coauthor of more than 50 journal publications and several book chapters on growth, fabrication, and characterization of wide bandgap semiconductor materials and nanostructures. He is the coauthor of a book titled *Zinc Oxide: Fundamentals, Materials and Device Technology* (New York, NY: Wiley, 2009).

Dr. Özgür is a member of the American Physical Society.

Daniel Hofstetter was born in Zug, Switzerland, in 1966. From 1988 to 1993, he studied physics at the Swiss Federal Institute of Technology (ETHZ), Zurich, Switzerland. In his diploma thesis under the supervision of Prof. Dr. F. K. Kneubuehl, he carried out photoacoustic spectroscopy on fatty acids using gas lasers. He received the Ph.D. degree from the Paul Scherrer Institute, Zurich, Switzerland, in 1996, for work which included the design, fabrication, and testing of a semiconductor-based monolithically integrated Michelson interferometer for optical displacement measurement.

After an apprenticeship as an Electrical Mechanic at Landis & Gyr, Zug, Switzerland, from 1982 to 1986, he became a Physics Technician until 1988. Later, he worked at the XEROX Palo Alto Research Center, Palo Alto, CA, developing single-mode InGaN-based violet semiconductor lasers (1996–1998). From 1998 to 2001, he was with the Mesoscopic Physics Group of Prof. Dr. Jerome Faist at the University of Neuchatel, Neuchatel, Switzerland, where his work concentrated on the fabrication and testing of single-mode distributed-feedback quantum-cascade (QC) lasers and high-performance QC lasers. From 2002 until now, he has been an Assistant Professor at the University of Neuchatel. His main activities included the development of novel types of semiconductor-based devices, such as QC detectors, for the midinfrared wavelength region.

Dr. Hofstetter has been the recipient of the prize of the Swiss Physical Society (1997), the Sofja Kovalevskaja award of the Alexander-von-Humboldt Foundation, Germany, and a Professorship award of the Professorship Program of the Swiss National Science Foundation.

Hadis Morkoç received the B.S.E.E. and M.S.E.E. degrees from Istanbul Technical University, Istanbul, Turkey, in 1968 and 1969, respectively, and the Ph.D. degree in electrical engineering from Cornell University, Ithaca, NY, in 1975.

From 1976 to 1978, he was with Varian Associates, Palo Alto, CA, where he was involved in various novel FET structures and optical emitters based on then new semiconductor heterostructures. He held visiting positions at the AT&T Bell Laboratories (1978–1979), the California Institute of Technology, Pasadena, and Jet Propulsion Laboratory (1987–1988), and the U.S. Air Force Research Laboratories-Wright Patterson AFB as a University Resident Research Professor (1995–1997). From 1978 to 1997, he was with the University of Illinois, Urbana. In 1997, he joined the newly established School of Engineering, Virginia Commonwealth University, Richmond, VA.

Dr. Morkoç is a Fellow of the American Association for the Advancement of Science, a Life Fellow of the American Physical Society, and is an inactive Fellow of IEEE.